Long-Term *in Vivo* Clearance of Gadolinium-Based AGuIX Nanoparticles and Their Biocompatibility after Systemic Injection

Lucie Sancey,[*,#,†] Shady Kotb,[#,†] Charles Truillet,[†] Florence Appaix,[‡] Arthur Marais,[†] Eloïse Thomas,[†] Boudewijn van der Sanden,[‡] Jean-Philippe Klein,[§] Blandine Laurent,[§] Michèle Cottier,[§] Rodolphe Antoine,[†] Philippe Dugourd,[†] Gérard Panczer,[†] François Lux,[†] Pascal Perriat,[∥] Vincent Motto-Ros,[†] and Olivier Tillement[†]

[†]Institut lumière matière, UMR5306, Université Claude Bernard Lyon1-CNRS, Université de Lyon 69622 Villeurbanne cedex, France, [‡]GIN INSERM U836 UJF, Grenoble, 38706, France, [§]LINA EA 4624—Laboratoire Interdisciplinaire d'étude des Nanoparticules Aérosolisées, Saint Etienne, 42023, France, and [∥]MATEIS, UMR 5510 INSA Lyon—CNRS, INSA Lyon, 69621 Villeurbanne, France. [#]These authors contributed equally to this work.

ABSTRACT We previously reported the synthesis of gadolinium-based nanoparticles (NPs) denoted AGuIX (activation and guiding of irradiation by X-ray) NPs and demonstrated their potential as an MRI contrast agent and their efficacy as radiosensitizing particles during X-ray cancer treatment. Here we focus on the elimination kinetics of AGuIX NPs from the subcellular to whole-organ scale using original and complementary methods such as laser-induced breakdown spectroscopy (LIBS), intravital two-photon microscopy, inductively coupled plasma optical emission spectrometry (ICP-OES), transmission electron microscopy (TEM), and electrospray ionization mass spectrometry (ESI-MS). This combination of techniques allows the exact mechanism of AGuIX NPs elimination to be elucidated, including their retention in proximal tubules and their excretion as degraded or native NPs. Finally, we demonstrated that systemic AGuIX NP administration induced moderate and transient effects on renal function. These results provide useful and promising preclinical information concerning the safety of theranostic AGuIX NPs.

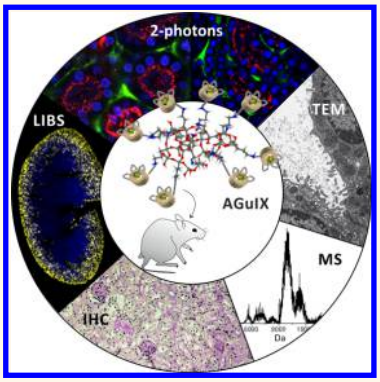

KEYWORDS: nanoparticle · gadolinium · theranostic · two-photon microscopy · laser-induced breakdown spectroscopy · renal function · toxicity

In the past two decades, the imaging and therapeutic capabilities of nanoparticles (NPs) have demonstrated high usefulness for biomedical applications.[1,2] Independent of their chemical composition, shape, or charge, most NPs between 20 and 200 nm are partially eliminated by the liver, contributing to retention within the reticuloendothelial system (RES), which includes macrophages and macrophage precursors, specialized endothelial cells that line the liver sinusoids, bone marrow, and spleen. Long-term retention of NPs could induce toxicity.[3−5] It is sensible to assume that biodistribution, accumulation, metabolism, and excretion of NPs will affect the toxicity of this nanoagent in the organism. The ability of the nanoparticles to affect the normal physiology as well as the normal structure of organs and tissues depends on physiochemical parameters such as particle size, shape, surface charge, chemistry, composition, and stability. Thus, research has focused either on the development of biodegradable NPs or on NPs with a hydrodynamic diameter (HD) smaller than 6 nm to prevent any undesired accumulation and promote renal clearance.[6,7] However, an HD smaller than the theoretical glomerular filtration limit (<6 nm)[8] may not be sufficient to promote glomerular filtration. Ultrasmall gold NPs (D < 2 nm) have been reported to be either mainly excreted through the liver several days after injection[9] or rapidly eliminated *via* the kidneys.[10]

* Address correspondence to lucie.sancey@univ-lyon1.fr.

Received for review August 2, 2014 and accepted February 21, 2015.

Published online 10.1021/acsnano.5b00552

Considering the use of MRI contrast agents, superparamagnetic iron oxide nanoparticles (SPIONs) or gadolinium-based MRI agents, the process of imaging should be a safe diagnostic procedure. SPIONs are often eliminated through both kidney and liver, which might lead to RES retention or migration of the particles through the organism.[11−13] This specific retention in the liver is sometimes the purpose of the SPION, dedicate to hepatic imaging. Nevertheless, the SPIONs family, including their byproducts, might trigger an immunological or an inflammatory response, processes that should be investigated before clinical transfer.[4,14] The gadolinium-based MRI contrast agents were approved by the FDA and European agencies in the early 2000s. Among them, some nanoparticles were correlated with high (>0.1 case/million applications) relative frequency of nephrogenic systemic fibrosis (NSF).[15−18] This serious and sometimes fatal disease has been related to transmetalation which leads to the release of free gadolinium from the chelates in the body, due to previous renal dysfunction, extensive administration of gadolinium, and/or coexistence of disease such as inflammation.[19] The transmetalation occurs particularly with acyclic chelates. Therefore, the guidelines issued by the regulatory authorities allowed a reduction of the number of new cases of NSF to almost zero; these guidelines include providing patients a possible benefit that outweighs the risk, limiting the amount of injected gadolinium, and measuring the glomerular filtration rate prior to the administration of Gd-chelate.[20]

We previously developed original polysiloxanes nanoparticles containing gadolinium ions (Gd) called AGuIX (activation and guiding of irradiation by X-ray) NPs, with an HD of approximately 3 nm for therapeutic application including radiosensitization and multimodal imaging.[2,21−23] The process of elimination and safety of AGuIX NPs has to be evaluated as a part of the preclinical evaluation. AGuIX NPs are mainly eliminated through the kidneys. Twenty-four hours after injection, less than 0.2% of the injected dose of radiolabeled particles was observed in any other organ.[2,24−26] However, the mechanism of AGuIX elimination remained unclear. To determine the exact mechanism underlying of AGuIX elimination, the study was determined in a mice model. The AGuIX NPs were administered intravenously (IV) to mice prior to investigation of renal function. Using either native or fluorescently labeled particles, we combined intravital and fixed-sample explorations at the subcellular to whole-organ scale using two-photon microscopy, inductively coupled plasma optical emission spectrometry (ICP-OES), transmission electron microscopy (TEM), and a method we have developed for biological tissue application, laser-induced breakdown spectroscopy (LIBS). Exposure to Gd-containing agents was associated with the occurrence of NSF; such pathology might be due to the release of Gd from the agent and seems to occur for acyclic agents.[27] However, the AGuIX NPs possess cyclic chelating agents and exhibit a very strong complexation constant ($\log\beta_{110} = 24.78$), which prevent Gd release.[21] In this study, we analyzed renal function, identified the NP's metabolites in urine samples by electrospray ionization mass spectrometry (ESI-MS), and obtained evidence of the safe biodegradation of the NP *in vivo*. In addition, histological analysis of kidney sections performed after repeated treatment with AGuIX confirmed the low impact of multiple injections on renal function and microstructure.

PRELIMINARY RESULTS: BRIEF DESCRIPTION OF THE NANOPARTICLE

The Gd-based AGuIX NPs were developed and designed for theranostic approaches in cancer radiotherapy.[2,21,23] AGuIX NPs are composed of a polysiloxane network surrounded by Gd chelates covalently grafted to the polysiloxane inorganic matrix and are synthesized by a top-down process (Figure 1A and Supporting Information).[2,21] These NPs exhibit an ultrasmall size, with an HD of approximately 3 ± 0.1 nm (Figure 1B). The complexation constant ($\log\beta_{110}$) of these NPs for Gd is 24.78.[21] This value is very close to the complexation constant of the commercial agent DOTAREM (25.58) determined under the same conditions. AGuIX NPs contain approximately 10 chelates per NP, with a mass of approximately 9 kDa. A representative MS measurement and the corresponding deconvolution of native full NPs are shown in Figure 1C.[28] In human serum, the particles are slowly degraded with time, in a dose-dependent manner, until reaching an equilibrium of stability (Figure 1D). This partial degradation occurs on the polysiloxane matrix level, with the hydrolysis of the Si−O−Si bonds and without releasing any of the gadolinium ions.[28]

RESULTS

I. AGuIX Renal Kinetics and Mechanism of Elimination. Previous studies of the Gd-based AGuIX NP indicated both rapid kidney accumulation and renal clearance of the particles, as expected for their small size.[2,25,29] Twenty-four hours after intravenous (IV) injection, a fraction of the injected dose (ID, approximately 10% ID/g) was still observed in the kidney, whereas all other organs exhibited less than 0.2% of the total ID. Different techniques employing both native and fluorescently labeled NPs were employed to precisely investigate and understand the renal elimination of AGuIX NPs after injection of a therapeutic dose (8 μmol of Gd in mice). These techniques present simultaneously advantages and drawbacks (see Supporting Information, Table S1) as well as different resolutions and sensitivities, resulting in a strong complementarity.

Whole-Organ Imaging Using Laser-Induced Breakdown Spectroscopy (LIBS). LIBS scanning imaging studies

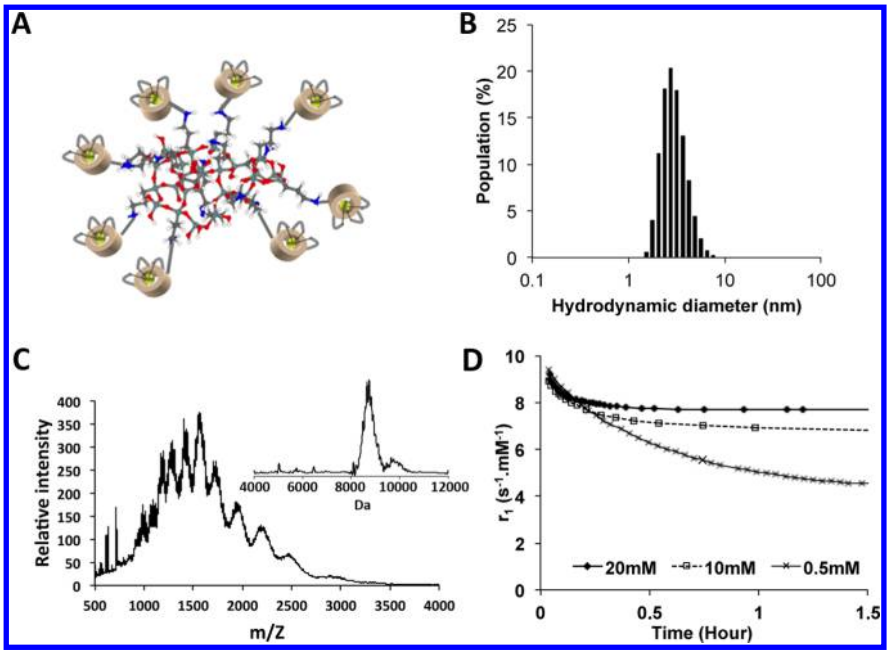

Figure 1. Gd-based AGuIX NP. (A) The components of AGuIX NPs are schematically represented as follows: Gd atoms chelated by DOTA derivatives are indicated in green, and the polysiloxane matrix comprising mainly silicon and oxygen is indicated in gray and red, respectively. The average molecular mass of a AGuIX NP is 8.7 ± 0.3 kDa, with a high Gd content (15 wt %). AGuIX NP has an average chemical formula $Gd_{10}Si_{40}C_{200}N_{50}O_{150}H_x$. (B) The HD distribution of AGuIX NPs as determined by DLS indicates a size of 3 nm. (C) ESI-MS measurements as recorded on the global spectrum. The inset indicates the spectrum generated after deconvolution with a multiplicative correlation algorithm. (D) Temporal evolution of the longitudinal relaxivity (r_1) of the particles, related to their stability, in human serum. The curve fittings, represented by lines, were determined by a monoexponential decay model.

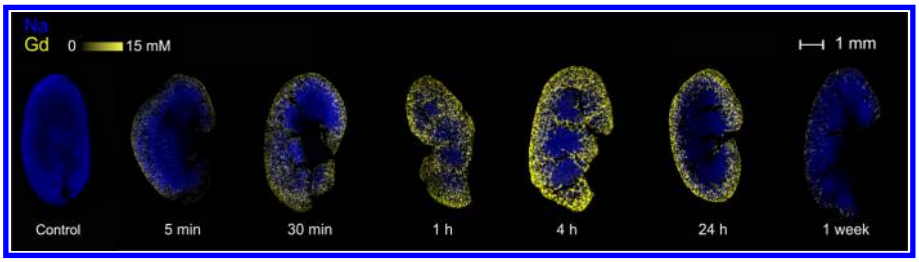

Figure 2. Quantitative imaging of Gd and sodium (Na) by LIBS, related to the distribution of AGuIX NPs in the kidney as a function of elapsed time after administration. Images have been recorded with a spatial resolution of 40 μm. See also Supporting Information, Table S1.

were first performed at the entire organ scale. Label-free NPs were injected IV in mice. Kidneys were subsequently collected, epoxy-embedded, and sliced for LIBS analysis. We recently adapted this technique to image and quantify multichemical elements in biological tissues (see Supporting Information, Figure S1).[30−32] This novel approach possesses an all-optical design and allows multielemental scanning imaging and quantification with a maximal spatial resolution of 10 μm.

To evaluate the kinetics of AGuIX NP elimination, kidneys were collected at different elapsed times after AGuIX NP administration (ranging from 5 min to 1 week) and imaged for Gd, a major element of AGuIX NPs (Figure 2). AGuIX NPs rapidly reached the kidneys, as indicated by the detection of the Gd signal as early as 5 min after IV injection, indicating that the NPs were distributed throughout the organism and reached the kidney during the first passage of blood through the organ. As for all components filtered by the kidneys, AGuIX NPs were first observed in close proximity to the cortex region, where the Bowman's capsules are located and in excellent agreement with previous nuclear imaging studies,[2] before diffusing throughout the entire organ (see Supporting Information, Figure S2). The elimination process resulted in the production of an increasing Gd signal that reached a maximum at 4 h postadministration, followed by a subsequent decrease. One week after injection, most of the signal had been cleared, indicating effective particle elimination from the body *via* urine. One week after IV injection, a weak Gd signal was still observed; this could be attributable to a specific entrapment of the particles in the tubules. We also performed high-resolution screening of a kidney sampled 3 h after IV injection of AGuIX NPs. As indicated in Figure 3, the Gd signal was heterogeneous in the cortex region, suggesting a specific accumulation in this region.

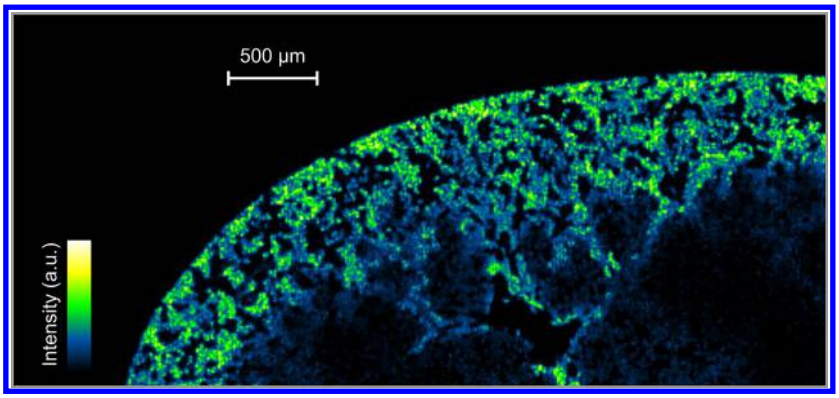

Figure 3. High-definition image of Gd obtained by LIBS. The kidney was screened with a spatial resolution of 10 μm (80 000 pixels), currently the highest resolution that might be obtained using LIBS. The heterogeneous distribution of Gd in the kidney cortex is readily apparent 4 h postinjection.

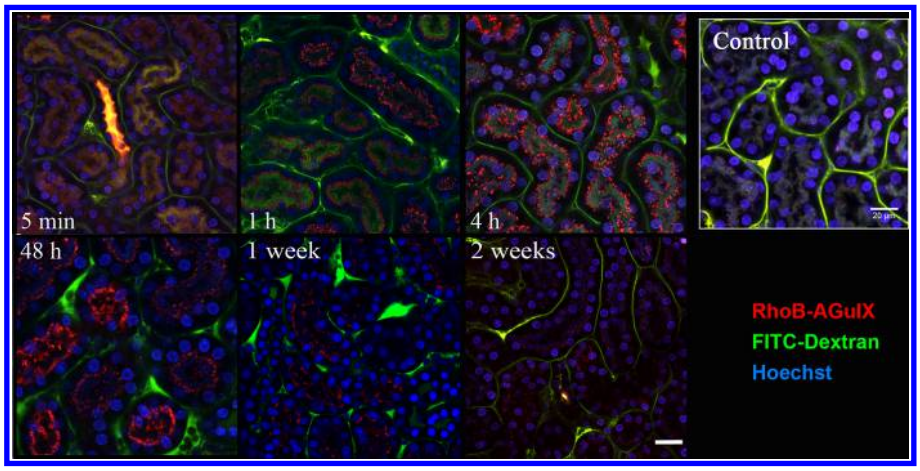

Figure 4. Two-photon microscopy of mice kidneys, from 5 min to 2 weeks after a single injection of 200 μL of Rhodamine B-AGuIX (red) at 40 mM Gd. The nucleus and vessels were stained by injecting 50 μL of a mixture of Hoechst 33342 (blue) and FITC-Dextran 70 kDa (green) 5 min before acquisition. The control condition was obtained after injection of staining mixture only (Hoechst 33342 and FITC-Dextran). Scale bar: 20 μm. Also see Supporting Information, Figure S5 for 5 min to 1 h *in vivo* kinetics.

Dynamic Approach of the Cortex Uptake. To prevent the use of fixative during the determination of the elimination kinetics, we used intravital two-photon microscopy analysis of functional kidneys. Intravital two-photon microscopy is a high-resolution, real-time, fluorescence imaging technique that permits the analysis of structural and functional changes in a given tissue at the single cell to the millimeter level.[33,34] To visualize the renal elimination of the NPs, fluorescent Rhodamine B-labeled AGuIX NPs were injected IV in mice 5 min to 2 weeks prior to two-photon microscopy imaging. During anesthesia, the kidney was maintained in a humidified environment at 37 °C outside the mouse body to eliminate movement due to breathing and maintain kidney function and blood circulation and placed under the microscope objective (see Supporting Information, Figure S3). A mix of fluorescent dyes was also injected IV to better localize both nuclei and vessels (counterstaining).

Rhodamine B-labeled AGuIX NPs reached the kidney as soon as 5 min after injection, as indicated by a diffuse red signal observed in both the blood vessels and the tubules (Figure 4). In vessels, the colocalization of FITC-dextran (70 kDa; green) with Rhodamine B (red) produced a high yellow signal. The NPs were rapidly extravasated and reached the tubules 1 h after injection, as indicated by precise red spots inside the tubule cells. For all investigations performed after longer than 1 h postinjection, a negligible signal was detected in the nuclei and the vessels, indicating efficient filtration of the particles. Similar results were observed at 4 and 48 h postinjection, with a high red fluorescent signal in the cytoplasm of tubule cells. At all time points between 1 and 48 h, some of the tubules appeared to contain the highest number of particles, as previously observed by LIBS; however, without more specific labeling, intravital microscopy analysis could not reveal whether this uptake was predominant in the proximal or distal convoluted tubules. One week after administration, AGuIX was poorly detected in some tubules, whereas others appeared completely empty. The renal elimination of AGuIX by 2 weeks after injection was indicated by a very weak red signal similar to that observed in the control (Supporting Information, Figure S4a).

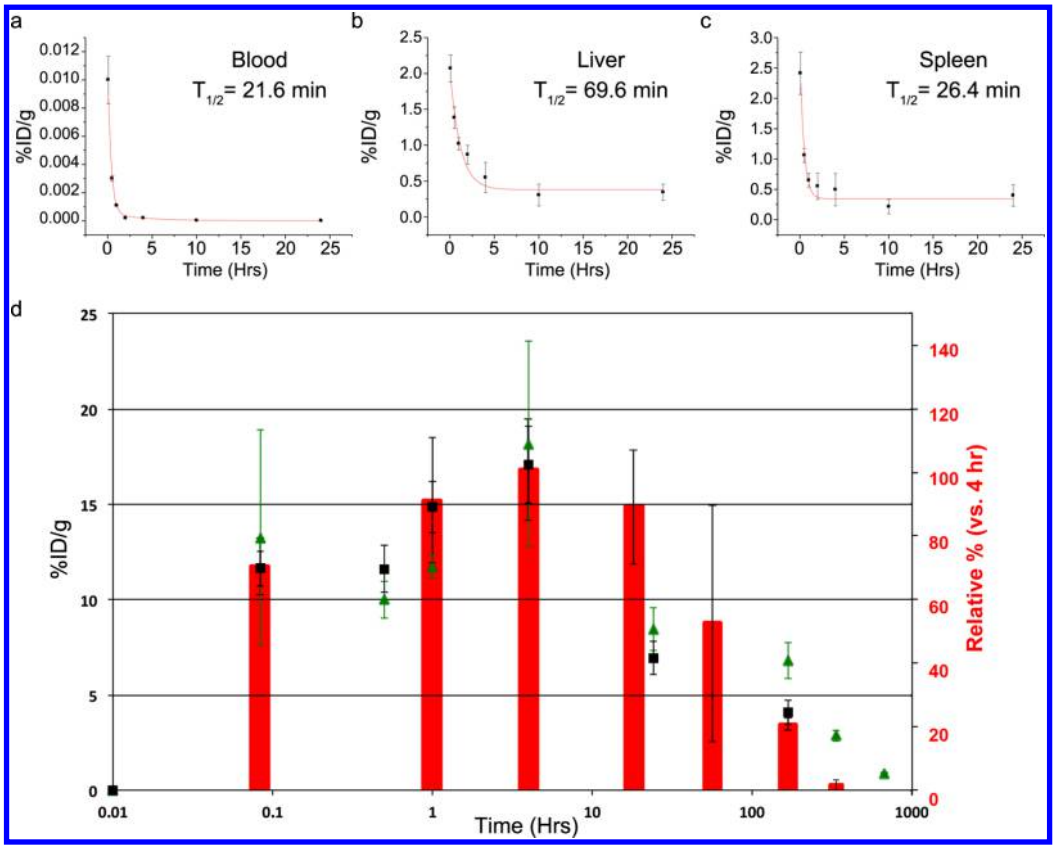

Figure 5. Evaluation of nanoparticle's kinetics of distribution. The nanoparticle's half-life was determined in (a) blood, (b) liver, and (c) spleen. (d) Direct comparison of the quantitative and relative data obtained after LIBS (black), and ICP-OES (green) experiments (both expressed as %ID/g) or two-photon microscopy (relative % *vs* 4 h, red), for kidney.

Replacement of Rhodamine B with FITC had no effect on the kinetics (also see Supporting Information, Figure S4b).

Nanoparticle's Pharmacokinetic. The elimination kinetics were quantified in the blood, the liver, the spleen, and the kidneys (Figure 5). The biodistribution profiles of the kidney obtained by LIBS and intravital microscopy were also compared to the ones obtained by inductively coupled plasma-optical emission spectrometry (ICP-OES). As demonstrated by Figure 5d, the kinetics of uptake and elimination determined by two-photon microscopy and LIBS were in accordance with the values determined by ICP-OES.[35] For more representative results, ICP-AES was used to analyze the kidneys of three animals, including the contralateral kidney of the kidney used in the LIBS experiments.

The kinetics of accumulation and elimination determined by the three methods were in accordance and indicated a rapid inflow of AGuIX as soon as 5 min postinjection, a maximum peak after 4 h and a slow decrease until quasi-complete elimination 2 weeks after injection. Prior sample preparation was required prior to the LIBS experiments, including vascular perfusion of the kidney by a fixative that removed and replaced the blood. This step might explain the difference observed in the first minutes postinjection. One and two weeks post injection, the data obtained by two-photon microscopy and ICP-OES were significantly different, possibly due to the limitations of fluorescence microscopy, that is, the analysis of the surface of the kidney (300 μm depth), autofluorescence of the tissue, and high probability of enzymatic degradation of the labeled particle compared to the high sensitivity of the ICP-OES method. At 48 h postinjection, two-photon microscopy analysis revealed a heterogeneous distribution of AGuIX NPs, as indicated by a very high standard deviation (Figure 4). Nevertheless, the kinetics observed using the three different methods were highly comparable and complementary.

Investigation at the Cell Level Using Transmission Electron Microscopy (TEM). As observed in the previous experiments (Figures 3 and 4), some tubules retained particles for several days, whereas others tubules did not. To identify the type of convoluted tubules implicated in this specific retention in the renal cortex, TEM was used to analyze samples collected 5 min to 2 weeks postinjection. As demonstrated in Figure 6, a large quantity of particles was detected as early as 5 min after IV injection in both proximal and distal convoluted tubules. Similar results were observed 1 h after AGuIX NP administration. The samples collected 1 week after IV injection revealed a smaller quantity of particles, as indicated by the small number of vacuoles present in the proximal tubules, whereas in the distal tubules, particles were rarely detected. This

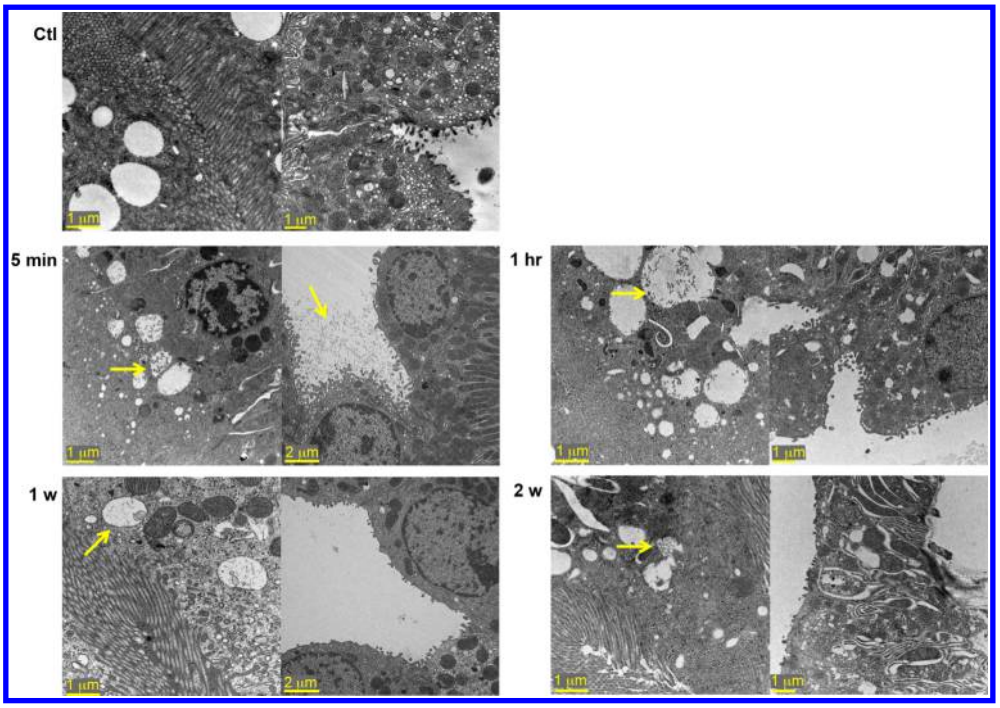

Figure 6. TEM images of the distribution of AGuIX NPs in the proximal (left panels) and distal convoluted tubes or glomerular region (right panels) as a function of elapsed time since a single injection. AGuIX particles are indicated by the arrows. At 2 weeks, few particles remained, and most of the observed regions were vacant. (See also Supporting Information, Figure S6 for a more detailed figure.)

specific retention in the proximal tubules under physiological conditions has been described, and the filtration process may occur for several days before excretion.[36] Finally, 2 weeks after injection, limited AGuIX aggregates were observed, although most of the particles were eliminated from both the proximal and distal tubules.

In summary, the results obtained by the different techniques used to determine the kinetics of AGuIX NP elimination were similar and indicated a rapid accumulation of AGuIX NPs in the kidneys from the first minutes to approximately 4 h postinjection. This accumulation was mainly observed in the proximal convoluted tubules, where some particles remained entrapped for several days after IV injection before excretion in urine.

II. AGuIX NP Biodegradation and Toxicity Studies. *IIa. Nanoparticle Metabolism.* On the basis of the results of the previous investigations, we can hypothesize that either (i) AGuIX NPs are eliminated as full native NPs from the body without any degradation or (ii) they are degraded in a long, specific process involving the proximal tubules. We performed mass spectrometry analysis of mouse urine to elucidate the process of degradation and evaluate this hypothesis. The urine was either withdrawn from the bladder to obtain the first 24 h samples or collected over 24 h beyond this time (n = 3 minimum/point). The relative intensity of the total ion signal recorded on the mass spectrometer ion detector was recorded as a function of time (Supporting Information, Figure S7). The deconvolution of the ESI spectra (Figure 7A) revealed two main distributions of NPs at 8.75 kDa (±320 Da) and 9.6 kDa (±670 Da), as well as several secondary distributions corresponding to the macromolecules observed at 4 and 7.7 kDa. At low mass (<8 kDa), the macromolecules, which were identified by their isotopic distribution (Supporting Information, Figure S6, inset), corresponded perfectly with those obtained from artificially degraded NPs[28] and were mainly observed 5 min postinjection of AGuIX NPs before strongly decreasing with time (Figure 7A). From 5 min to 4 weeks post-IV injection, the full native AGuIX NPs were present in the urine. A mathematical deconvolution of the mass spectra associated with the NPs brings to light two distribution masses, one observed at 8.75 kDa and the second at 9.6 kDa. The smallest NPs corresponding to 8.75 kDa were eliminated more rapidly than those constituting the 9.6 kDa population, as indicated by the decrease in their relative intensities with time; this result indicates that the elimination of NPs is related to their mass. After 4 weeks, the very weak signal measured by mass spectrometry still corresponded to the signal of the native AGuIX NPs, indicating that some particles remained in the kidneys.

A comparison of the results obtained by mass spectroscopy and ICP-OES was performed (Figure 7B). The relative quantity of AGuIX NPs quantified in the urine by mass spectrometry perfectly matched the quantity of particles measured by ICP-OES when standardized to 4 h postinjection. Thus, the NPs that enter the kidney may be excreted in comparable proportions.

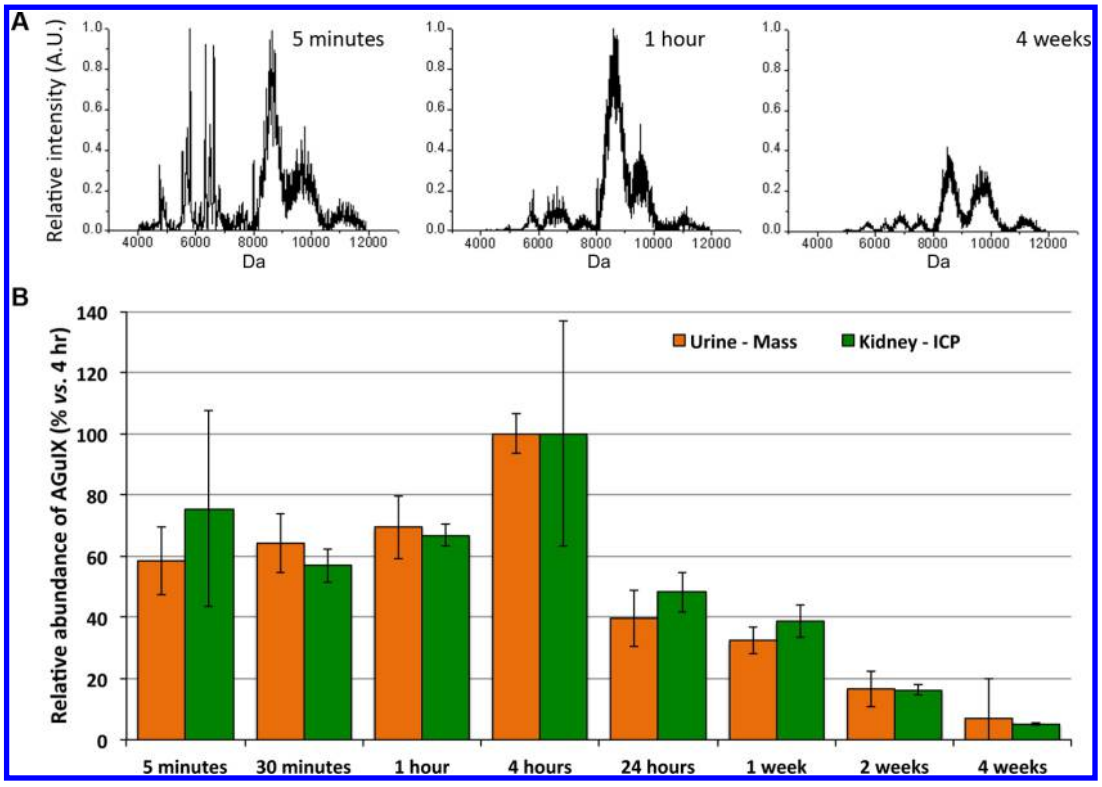

Figure 7. Urine analysis by mass spectroscopy after IV injection of AGuIX NPs. (A) Deconvoluted ESI mass spectra from *m/z* spectra of urine samples collected at 5 min, 1 h, and 4 weeks after a single injection of AGuIX NPs, expressed as mass (Da). (B) Comparison of the relative quantities of AGuIX NPs measured in the urine by mass spectrometry and ICP-AES.

TABLE 1. Serum Creatinine Concentration after a Single Injection of AGuIX NPs (8 μmol/mouse), Expressed as mg/L $\pm$ SD[a]

	control	5 min	30 min	1 h	4 h	24 h	1 week	2 weeks	4 weeks	8 weeks
Creatinine level	8.7 $\pm$ 0.5	8.0 $\pm$ 1.7	12.7 $\pm$ 2.2*	6.5 $\pm$ 3.5	7.8 $\pm$ 1.8	5.5 $\pm$ 0.2	6.4 $\pm$ 1.4	7.0 $\pm$ 1.3	8.7 $\pm$ 0.4	8.5 $\pm$ 2.0

[a] The concentration was measured using the Jaffé method and compared to that measured in control mice (n = 3).

During the elimination process, small degraded particles were eliminated from the body in the first minutes postinjection, whereas full native AGuIX NPs were entrapped in the proximal convoluted tubules from a few hours to several days before elimination from the organism as native AGuIX NPs.

IIb. Evaluation of Safety: Renal Function and Maximum Tolerated Dose (MTD). An evaluation of global toxicity is necessary prior to the clinical application of a compound. In the present context, the fine evaluation of renal function is crucial to confirm the absence of side effects in this major elimination organ. Renal function was evaluated based on serum creatinine levels and histological analysis of the kidneys after different elapsed times post AGuIX administration. A study of MTD was also conducted to determine the main observable effects of AGuIX on mice after bolus injection.

Renal function was first evaluated by measuring serum creatinine concentrations.[29,37] As shown in Table 1, the serum creatinine concentration was significantly increased 30 min after NP administration (p = 0.042), but the serum level returned to physiological levels as soon as 1 h after IV injection, indicating a transient perturbation that may be attributable to the bolus injection of the particles.

A histological study of the kidney was then performed after three repeated injections of AGuIX NPs (1 injection per week for 3 weeks) to determine the impact of multiple injections on renal function at the microscopic scale. Standard periodic acid-Schiff (PAS) staining was used to identify structural modifications, the presence of infiltrate cells and glomerular fibrosis. As shown in Figure 8, after three consecutive IV administrations of AGuIX NPs, some tubular vacuoles appeared (+2 weeks). This slight modification might be transient and insignificant. To assess the reversibility of this phenomenon and study the long-term impact of AGuIX NPs administration, kidneys were collected 4 and 8 weeks after treatment and analyzed by PAS staining. Neither atrophic tubules nor necrotic cells were observed in the tubules. Some focal vacuoles appeared without necrosis but decreased with time (+8 weeks). Local abrasion of the brush border (+2 weeks) was completely repaired after 4 weeks. For all samples, staining in the glomeruli indicated the

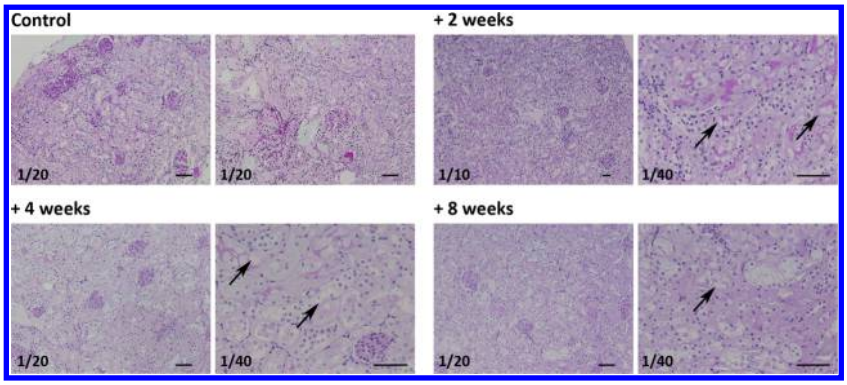

Figure 8. PAS staining of renal sections after repeated injection of AGuIX NPs (1 injection every week for 3 weeks). The arrows indicate tubular vacuoles. The magnification is indicated at the left bottom corner of each image. Scale bar: 50 μm.

TABLE 2. Determination of the MTD of AGuIX in Non-tumor-bearing Mice after a Single IV Injection[a]

dose/inj	AGuIX NPs concn	experimental state score (ESS)					wt variation	
μmol/mouse	g/L	diarrhea	lethargy	closed eyes	difficulty waking after anesthesia	total	%	no. of deaths
30	150	0	0	0	0	0	+3.2	0
40	200	0	0	0	1	1	+5.4	0
50	250	0	0	0	2	2	+0.8	0
75	500[c]	0	0	0	3	3	+0.5	1[b]

[a] The ESS was calculated based on the absence (0) or presence (1) of the evaluated settings. The total ESS was calculated by summing the individual scores. [b] Death occurred a few seconds after bolus injection. [c] Injected volume = 150 μL.

absence of lesions, absence of cell proliferation, and absence of deposits. At the vessel level, no lesions were observed. The interstitial tissue indicated the absence of fibrosis or edema, a limited number of inflammatory cells (<1%, see also Supporting Information, Figure S8) and some peritubular dilated capillaries containing erythrocytes. In summary, the observed modifications were slight and transient after three consecutive injections of AGuIX NPs.

Finally, a specific study was performed to evaluate the MTD of AGuIX NPs. AGuIX NPs were IV injected into six mice per group, and the mice were followed for 10 days to detect any adverse effects (Table 2). For *in vivo* applications in mice, the therapeutic dose (TD) corresponds to an injection of 8 μmol of [Gd^{3+}] (a volume of 200 μL at a concentration of 40 mM [Gd^{3+}]). The TD is defined as the quantity of Gd per body mass mostly used in clinical MRI applications. Increasing doses in the same volume were IV injected in mice to determine the MTD, which is defined as the highest single dose of AGuIX NPs that does not cause any animal fatalities in a group, a maximal weight loss of 10% of total body weight at the end of the experiment, and the smallest experimental score, as defined in Table 2. For single doses, no death was observed 10 days after AGuIX NPs injection, maximal weight losses were less than 10% of total body weight, and the experimental state scores (ESS) were low, even at doses 10-fold higher than the intended safe dose. Thus, a dose 10-fold higher than the TD could be used before fatalities occurred. In these experiments, colloidal AGuIX NP solutions with a concentration of 500 g/L, the highest concentration at which the particles were soluble, were injected *via* a bolus.

These first results of the investigations of the safety of AGuIX NPs indicate promise for translation to the clinic. The very weak observed effects transiently altered renal function, as indicated by serum creatinine levels and the repair of tubular vacuolation within several weeks after repeated treatment. The MDT in mice was nearly 10-fold higher than the TD after bolus injection; slow IV injection may increase tolerance. Taken together, these results indicate promise for future regular studies of AGuIX NPs.

DISCUSSION AND CONCLUSION

The 3 nm Gd-based AGuIX NPs were previously developed and designed for theranostic approaches in cancer radiotherapy. In parallel with investigations of efficacy, preliminary *in vivo* safety studies are required to determine their pharmacokinetics, elimination pathway, metabolism, and potential degradation.

The rapid renal elimination of AGuIX NPs after IV administrations was confirmed and characterized in this study.[2,26,35] The retention of AGuIX NPs in the renal cortex and their clearance was demonstrated by LIBS elemental imaging. This innovative method can map and precisely quantify several elements, including Gd, one of the main constitutive elements of the particles. The heterogeneous distribution of Gd in the cortex was

also determined by a high-definition investigation (Figure 3). Intravital two-photon microscopy revealed fast renal entry of the particles,[38] following the first heartbeats. This method also indicated that the highest uptake occurred 4 h after administration and that tubular retention was heterogeneous, particularly 48 h after administration (Figure 4). The fluorescent signal was mainly lost 2 weeks after IV injection, possibly due to partial degradation of the labeled particles and consequent dye excretion and/or the limitation of the technique itself, as some native particles were still detected by the ICP-OES method. Spectrometric methods, i.e., ICP-OES and LIBS, confirmed these kinetics but also generated quantitative information for either the entire kidney or kidney sections. The fine sensitivity of ICP-OES enabled the detection of particles several weeks after administration; only 0.5% of the injected dose was measured in the kidney 4 weeks after IV injection. These three methods provided similar but complementary information about AGuIX NPs elimination due to their different sensitivities and biological scales.

The comparison of the different methods revealed high standard deviations (SD) for ICP-OES in the first hours after IV administration; this SD might be due to the presence of particles in the bloodstream or diuresis (Figure 5). By contrast, the high SD measured by two-photon microscopy at 48 h post-IV injection demonstrated the heterogeneity of the distribution of AGuIX NPs between proximal and distal tubules. Thus, more than 95% of the particles were efficiently eliminated within the first week after IV administration, with approximately 99% removal after 4 weeks. These rates of removal are consistent with the pattern of elimination of other small, silicon-based particles: major elimination in the first days and complete elimination after several weeks.[6,7,39,40] We were able to determine precisely the different byproducts excreted from the body in urine. The first excreted products corresponded to both degraded AGuIX NPs that were most likely biodegraded after dilution in the bloodstream and entire particles, whereas only intact particles were released after a couple of minutes. This pattern of biodegradation and elimination favors safe elimination of the compound.

TEM revealed renal accumulation of AGuIX NPs in the proximal tubules, whereas the distal tubules were rapidly cleared. The functions of the proximal tubule cells include the degradation of compounds after glomerular filtration by exposure to low pH (pH 4 in lysosomes) and return of the byproducts, consisting of a piece of polysiloxane surrounded by chelating moiety and Gd, to the bloodstream or elimination through urine. The long accumulation of AGuIX NPs in these cells might be explained partially by the high stability of AGuIX NPs in acidic medium, which prevents their degradation in lysosomes before their elimination in urine.[41] However, a single bolus injection was very well tolerated in rodents, even at high concentrations, as indicated by the MDT assay.

Histological analysis indicated that repeated injections led to transient vacuolation of the proximal convoluted tubules, a phenomenon that was mainly restored 8 weeks after a 3-week treatment. Renal tubules have a regenerative capacity;[42] however, the turnover of proximal tubule cells in adult rodents is very low, and less than 20% of the proximal tubule cells may regenerate during a 2 week period.[43] AGuIX NPs, which were efficiently eliminated, exerted a moderate and transient effect on proximal cells. The restoration of the proximal convoluted tubules may be due to self-repair as well as natural turnover.

To conclude, AGuIX Gd-based NPs, designed for theranostic applications in radiosensitizing cancer treatment, are eliminated *via* the urinary route in a two-step process involving rapid elimination of biodegraded and smaller particles and slower elimination of larger particles. The effect of AGuIX NPs on renal function was limited to the vacuolation of the proximal tubules cells; this phenomenon was moderate, transient, and did not affect renal function itself. All together, these results indicate the appropriate elimination of NPs from the organism, which is a prerequisite for the clinical development of such agents. In this paper, we combine different analytical methods to identify, image, and quantify the NPs *in vivo* and *ex vivo*. The interest of such a combination of imaging techniques and analytical measurements may be useful in nanomedicine with a wide range of materials that may be distinct from the background, especially for LIBS imaging. In particular, the correlation between analytical measurements and imaging of the compound of interest appear to be a good standard operating procedure in nanopharmacology and nanotoxicology, and may be exploited in different organs as a milestone protocol for distribution, accumulation/elimination, and toxicity of a wide range of NPs and materials in both physiological and pathological conditions.

MATERIAL AND METHODS

Chemicals and Reagents. The fluorescent dyes used for two-photon microscopy were fluorescein isothiocyanate (FITC)-dextran 70-kDa (50 mg/mL in saline, No. FD70S-1G, Sigma-Aldrich, Saint-Quentin Fallavier France) and Hoechst 34580 (Life Technologies SAS, Saint Aubin, France). Diethylene glycol (DEG, 99%) was purchased from SDS Carlo Erba (France). DOTAGA (1,4,7,10-tetraazacyclododecane-1-glutaric anhydride-4,7,10-triacetic acid) was furnished by Chematech (Dijon, France). Gadolinium chloride hexahydrate ([$GdCl_3$, 6 H_2O], 99%) and gadolinium oxide cores were furnished by Nano-H S.A.S (Saint-Quentin

Fallavier, France). Only Elga Purelab Ultra water ($\rho > 18$ MΩ) was used to prepare aqueous solutions.

Synthesis of the Gd-Based AGuIX NPs. AGuIX NPs were synthesized as previously described.[21] Detailed information can be found in the Supporting Information.

Relaxometry. Relaxation time measurements were performed using a Bruker Minispec MQ60 NMR analyzer, operating at 1.4 T magnetic field.

Animals and Ethics. Six- to eight-week-old Balb/c and NMRI nude mice were purchased from Janvier, France. All mice were housed in a specific pathogen-free (SPF) environment, and procedures were performed in accordance with the Institutional Animal Care and Use Committee at the University of Lyon and Grenoble. The research involving animals was authorized under the agreement number (L. Sancey, Ph.D., permit number 38 09 22 and project in accordance with French Guidelines No. LS-2013-004). All efforts were made to minimize the number of animals used and their suffering during the experimental procedure. Animals were housed in cages with food and water ad libitum and a 12 h light/dark cycle at 22 ± 1 °C.

Anesthetized mice were injected with AGuIX NPs as follows: single administration, 200 μL at 40 mmol/L; repeated injections (for the histology study) a similar dose administered once each week for three weeks.

Laser-Induced Breakdown Spectroscopy. *Kidney Sample Preparation.* Mice were initially anesthetized with 4% isoflurane, and anesthesia was maintained with ~2% isoflurane. Gd-based NPs (AGuIX, 8 μmol of Gd) were IV injected into the mice under anesthesia. The kidneys were sampled at various times from 5 min to 1 week after injection and were embedded in epoxy, as described elsewhere.[22] In brief, after sampling, each kidney was perfused and fixed with 2% glutaraldehyde in 0.1 M sodium cacodylate buffer (pH of 7.4) overnight at room temperature to preserve both the tissue structure and the distribution of the particles. The samples were then rinsed three times for 15 min each in 0.2 M sodium cacodylate buffer. After washing, the samples were dehydrated in a series of ethanol solutions of increasing concentration, ending with propylene oxide. The samples were then embedded in EPON (1:1 mixture of diglycidyl ether and dodecenylsuccinic anhydride, density of 1.22 g/L). The sample surfaces were prepared using a microtome. For elemental quantification, standards containing AGuIX NPs were embedded in the same EPON resin, at five concentrations ranging from 1 to 40 mM. The powders were mixed with the resin (for a minimum of 4 h), warmed for 2 days (60 °C), and finally prepared using a microtome.

LIBS Settings. The instrumental setup was based on a homemade optical microscope that combined a LIBS laser injection line, a standard optical-imaging apparatus, and a three-dimensional motorized platform for sample positioning. The LIBS experiment has been described elsewhere,[35] and only its main features are described in the following. Quadruple Nd:YAG laser pulses of 266 nm with a duration of 5 ns and a 10 Hz repetition rate were focused onto the sample by a high-power 15× magnification objective (LMU-15X-266, Thorlabs). During the experiments, the sample was translated along 2 axes by an X−Y motorized stage. The measurements were performed at room temperature with argon gas flowing through the plasma region. During the sample scan, trigonometric surface positioning was used to compensate for any flatness anomalies and to accurately control the focalization distance (the objective-to-sample distance). A beam shutter was used to control the delivery of the laser pulse to the sample such that only one plasma plume was produced for each position in the sample. The light emitted by the plume was collected by a quartz lens with a focal distance of 2 cm and focused onto the entrance of an optical fiber bundle. The output of the fiber bundle was connected to a Czerny−Turner spectrometer equipped with a 1200-L/mm grating blazed at 300 nm and an intensified charge-coupled device (ICCD) camera (Shamrock 303 and iStar, Andor Technology). The ICCD camera was synchronized with the Q-switch of the laser, and the spectrum acquisition was performed with a delay of 300 ns and a gate of 3 μs. A spectral measurement range of typically 30 nm was accessible with a spectral resolution of approximately 0.15 nm. The laser energy was stabilized throughout the experiment using a servo control loop to ensure the long-term stability of the laser output. Customized software developed in the LabVIEW environment controlled the entire system and enabled the performance of automated sequences to scan the region of interest of the tissue sample with a specific lateral resolution.[30]

Intravital Microscopy—Two-Photon Microscopy. Two-photon microscopy was performed using a LSM 7 MP (Zeiss, Germany) equipped with a 20× water-immersion objective (NA 1.0; Zeiss) and ZEN 2010 software. Laser excitation was performed at 800 nm with a Ti:sapphire laser (Chameleon vision II; Coherent, UK) using a constant laser power of approximately 60 mW. Fluorescence emissions were detected simultaneously by three nondescanned photomultiplier tubes with a 492/SP25 nm filter (Semrock, US) for "blue" fluorescence emission, a 542/50 nm filter (Semrock, US) for "'green'" fluorescence emission, and a 617/73 nm filter (Semrock, US) for "'red'" fluorescence emission (Rhodamine B). The blue and green channels were collected for specific labeling of the nucleus (Hoechst 34580) and blood vessels (FITC (fluorescein isothiocyanate)−Dextran), respectively. Autofluorescence and second harmonic generation of biological structures could also be collected in the three channels owing to the presence of collagen, lectin, and elastin.

During *in vivo* two-photon microscopy, animals were anesthetized with 1−2% isoflurane in a 70% air, 30% O_2 gas mixture. Body temperature was maintained at 37 °C using a heating blanket. A small incision was made in the mouse's back to expose the kidney. After imaging the kinetic elimination of AGuIX NPs for 1 or 2 h, a mixture of FITC−dextran and Hoechst was IV injected. Ten minutes later, the kidney was removed either for *ex vivo* imaging or chemical fixation and/or freezing in pentobarbital, followed by storage in liquid nitrogen until further analysis.

Inductively Coupled Plasma Optical Emission Spectrometry (ICP-OES) Analysis. ICP-OES analysis was used to determine the Gd content in both the NPs themselves and the kidneys. After a single injection of mice with AGuIX NPs, the kidneys were dispersed in 5 mL of aqua regia (67% HNO_3/37% hydrochloric acid (w/w)) for 4 h at 80 °C. Subsequently, the samples were diluted with a HNO_3 5% (w/w) matrix to adjust the volume to 10 mL; the samples were then filtered (0.22 μm) and analyzed by ICP-OES at the lab or at the "Service Central d'Analyses du CNRS" (Solaize, France) to determine the elemental content with a precision of 2%. For calibration of the ICP-OES, single-element standard solutions were prepared by successive dilution in a HNO_3 5% (w/w) matrix from a 1000-ppm Gd standard acquired from SCP Science. Importantly, for comparison with the LIBS experiment, the right kidney of each animal was sectioned for imaging, and the left kidney of the same animal was used for ICP-OES.

Transmission Electron Microscopy. Sampled kidneys were fixed as described previously or LIBS analysis and postfixed in 1% osmium tetroxide in 0.1 M sodium cacodylate buffer for 1 h. After washing, the samples were dehydrated in an ethanol series of increasing concentrations, ending with propylene oxide. The samples were then embedded in EPON (1:1 mixture of diglycidyl ether and dodecenylsuccinic anhydride). Thin sections of approximately 70 nm were prepared with a Reichert Ultracut E ultramicrotome. The sections were observed using a Philips CM120 electron microscope operating at 120 kV.

Electrospray Ionization (ESI) Mass Spectrometry. Full-scan mass spectra were obtained using a linear quadruple ion trap mass spectrometer (LTQ, Thermo Fisher Scientific, San Jose, CA) with enlargement for the high 2000−4000 Th range. The NP solution was electrosprayed at a flow rate of 20 μL/min in positive ion mode.

Two different tunes were used: one for high mass observation (Tune 1 between 200 m/z and 4000 m/z) and the other for low mass (Tune 2 between 150 m/z and 2000 m/z). The low mass tune allowed us to study AGuIX fragments. Isotopic distributions of fragment ions were recorded using the zoom scan mode of the LTQ ion trap mass spectrometer. Because AGuIX NPs contain multiple groups capable of being ionized (e.g., Gd-DOTA complexes), the ESI source can produce highly charged ions. For those macromolecules that can sustain multiple charges, a distribution of charge states is often observed in

the mass-to-charge spectrum. This multiplicity of states gives rise to an "envelope" of peaks in the spectrum. Such a distribution of charges was observed in the *m/z* range 1000−4000 after electrospraying in positive mode a water solution containing AGuIX NPs. A multiplicative correlation algorithm (MCA) was used to estimate the mass of the NPs from the mass-to-charge spectra produced by ESI-MS.[44] The multiplicative correlation is designed to enhance the deconvoluted signal when the parent molecule is distributed into several charge states in the measured spectrum.

Creatinine Level. Total blood samples were collected from the right ventricular cavity. The serum was separated by centrifugation at 3000*g* for 10 min at 4 °C, and the creatinine concentration was analyzed according to the manufacturer's instructions (Bio-Merieux, Marcy l'Etoile, France). Briefly, 2-point kinetics mode was used to measure the red-orange complex formed with picric acid in alkaline medium according to the Jaffe method. *In vivo* TPLSM imaging was performed at the Two-Photon Microscopy Platform (GIS-IBiSA ISdV, Photonic Imaging Center - Grenoble Institute of Neuroscience). Measurements were obtained with a 50 scan UV−visible spectrophotometer (Varian Cary Eclipse).

Maximal Tolerated Dose. Groups of six mice received a single bolus injection of AGuIX NPs at doses ranging from 30 to 75 μmol, that is, a single IV injection of 150 to 200 μL at concentrations from 150 to 500 g/L. After being injected, the mice were weighed and observed every day to evaluate the general clinical state. For each animal, a score was calculated based on the absence (value 0) or presence (value 1) of diarrhea, lethargy, closed eyes, and difficulty waking after anesthesia. An experimental state score (ESS) was then calculated for each group by summing the individual scores. Loss of weight and mortality were also recorded. The MTD was defined as the highest single dose that met all of the following criteria: absence of death in the group, maximal weight loss of 10% in nontumor-bearing animals, and ESS value as low as possible.

Histology. Histology was performed on kidney samples after repeated injections of AGuIX NPs(1 injection/week for 3 weeks). Kidneys were sampled at the indicated time after injection. Kidneys were then fixed in a Japanese fixative at 4 °C for a minimum of 1 h; next, kidneys were washed in cacodylate sodium, dehydrated in pure acetone, and incubated in glycol-methacrylate (GMA) for 3 h before embedding in GMA containing 0.8% aniline propanol. Japanese fixative is a solution of 6% paraformaldehyde, 8.5% sodium cacodylate, 0.073% calcium chloride, and 0.2% picric acid, adjusted at pH 7.4.

Resin sections with a thickness of 2 μm were prepared and stained with periodic acid-Schiff (PAS) using standard protocols. Briefly, 2-μm slides were treated with 0.5% periodic acid for 10 min, washed with water, colored with Schiff stain for 20 min, rinsed again with water, and then counter-stained with Harris hematoxylin for 30 min. Sections were mounted with resinous mounting medium.

Conflict of Interest: The authors declare no competing financial interest.

Acknowledgment. The authors gratefully acknowledge the LABEX iMUST (ANR-10-LABX-0064) and PRIMES (ANR-11-LABX-0063) of Lyon 1 University within the programs "Investissements d'Avenir" (ANR-11IDEX-0007 and ANR-11IDEX-0063, respectively), operated by the French National Research Agency (ANR) within the project EMILI, the ANR Multimage ANR-12-RPIB-0010, as well as the Lyon Science Transfert, for financial support. We also heartily acknowledge the CTμ (A. Rivoire and C. Boule), F. Pelascini (CRITT Matériaux Alsace) for fruitful discussions and advice regarding epoxy samples and standards, and F. Rossetti for AGuIX synthesis.

Supporting Information Available: Synthesis of the NPs; kinetics of elimination; advantages and disadvantages of the different techniques. This material is available free of charge *via* the Internet at http://pubs.acs.org.

REFERENCES AND NOTES

1. Hainfeld, J. F.; Smilowitz, H. M.; O'Connor, M. J.; Dilmanian, F. A.; Slatkin, D. N. Gold Nanoparticle Imaging and Radiotherapy of Brain Tumors in Mice. *Nanomedicine* **2013**, *8*, 1601–1609.
2. Lux, F.; Mignot, A.; Mowat, P.; Louis, C.; Dufort, S.; Bernhard, C.; Denat, F.; Boschetti, F.; Brunet, C.; Antoine, R.; *et al.* Ultrasmall Rigid Particles as Multimodal Probes for Medical Applications. *Angew. Chem., Int. Ed.* **2011**, *50*, 12299–12303.
3. Cho, W. S.; Cho, M.; Jeong, J.; Choi, M.; Han, B. S.; Shin, H. S.; Hong, J.; Chung, B. H.; Jeong, J.; Cho, M. H. Size-Dependent Tissue Kinetics of PEG-Coated Gold Nanoparticles. *Toxicol. Appl. Pharmacol.* **2010**, *245*, 116–123.
4. Dufort, S.; Sancey, L.; Coll, J. L. Physico-Chemical Parameters that Govern Nanoparticles Fate also Dictate Rules for their Molecular Evolution. *Adv. Drug Delivery Rev.* **2012**, *64*, 179–189.
5. Han, S. G.; Lee, J. S.; Ahn, K.; Kim, Y. S.; Kim, J. K.; Lee, J. H.; Shin, J. H.; Jeon, K. S.; Cho, W. S.; Song, N. W.; *et al.* Size-Dependent Clearance of Gold Nanoparticles from Lungs of Sprague-Dawley Rats after Short-Term Inhalation Exposure. *Arch. Toxicol.* **2014**, 10.1007/s00204-014-1292-9.
6. Huang, X.; Li, L.; Liu, T.; Hao, N.; Liu, H.; Chen, D.; Tang, F. The Shape Effect of Mesoporous Silica Nanoparticles on Biodistribution, Clearance, and Biocompatibility *in Vivo*. *ACS Nano* **2011**, *5*, 5390–5399.
7. Choi, H. S.; Liu, W.; Misra, P.; Tanaka, E.; Zimmer, J. P.; Itty Ipe, B.; Bawendi, M. G.; Frangioni, J. V. Renal Clearance of Quantum Dots. *Nat. Biotechnol.* **2007**, *25*, 1165–1170.
8. Deen, W. M. What Determines Glomerular Capillary Permeability? *J. Clin Invest* **2004**, *114*, 1412–1414.
9. Semmler-Behnke, M.; Kreyling, W. G.; Lipka, J.; Fertsch, S.; Wenk, A.; Takenaka, S.; Schmid, G.; Brandau, W. Biodistribution of 1.4- and 18-nm Gold Particles In Rats. *Small* **2008**, *4*, 2108–2111.
10. Hainfeld, J. F.; Slatkin, D. N.; Focella, T. M.; Smilowitz, H. M. Gold Nanoparticles: A New X-ray Contrast Agent. *Br. J. Radiol.* **2006**, *79*, 248–253.
11. Gupta, A. K.; Gupta, M. Synthesis and Surface Engineering of Iron Oxide Nanoparticles for Biomedical Applications. *Biomaterials* **2005**, *26*, 3995–4021.
12. Laurent, S.; Forge, D.; Port, M.; Roch, A.; Robic, C.; Vander Elst, L.; Muller, R. N. Magnetic Iron Oxide Nanoparticles: Synthesis, Stabilization, Vectorization, Physicochemical Characterizations, and Biological Applications. *Chem. Rev.* **2008**, *108*, 2064–2110.
13. Morana, G.; Salviato, E.; Guarise, A. Contrast Agents for Hepatic MRI. *Cancer Imaging* **2007**, *7* Spec No A, S24−S27.
14. Markides, H.; Rotherham, M.; El Haj, A. J. Biocompatibility and Toxicity of Magnetic Nanoparticles in Regenerative Medicine. *J. Nanomater* **2012**, 614094.
15. Heverhagen, J. T.; Krombach, G. A.; Gizewski, E. Application of Extracellular Gadolinium-Based MRI Contrast Agents and the Risk of Nephrogenic Systemic Fibrosis. *R. College Radiol.* **2014**, *186*, 661–669.
16. Thomsen, H. S.; Morcos, S. K.; Almen, T.; Bellin, M. F.; Bertolotto, M.; Bongartz, G.; Clement, O.; Leander, P.; Heinz-Peer, G.; Reimer, P.; et al. Nephrogenic Systemic Fibrosis and Gadolinium-Based Contrast Media: Updated ESUR Contrast Medium Safety Committee Guidelines. *Eur. J. Radiol.* **2013**, *23*, 307–318.
17. Perazella, M. A. Nephrogenic Systemic Fibrosis, Kidney Disease, and Gadolinium: Is There a Link? *Clin J. Am. Soc. Nephrol.* **2007**, *2*, 200–202.
18. Deo, A.; Fogel, M.; Cowper, S. E. Nephrogenic Systemic Fibrosis: A Population Study Examining the Relationship of Disease Development to Gadolinium Exposure. *Clin J. Am. Soc. Nephrol.* **2007**, *2*, 264–267.
19. Jalandhara, N.; Arora, R.; Batuman, V. Nephrogenic Systemic Fibrosis and Gadolinium-Containing Radiological Contrast Agents: An Update. *Clin. Pharmacol. Ther.* **2011**, *89*, 920–923.
20. *Advisory, F.P.H. Gadolinium-Containing Contrast Agents for MRI*; Faculty of Public Health: London, **2006**.
21. Mignot, A.; Truillet, C.; Lux, F.; Sancey, L.; Louis, C.; Denat, F.; Boschetti, F.; Bocher, L.; Gloter, A.; Stephan, O.; *et al.* A Top-Down Synthesis Route to Ultrasmall Multifunctional

Gd-Based Silica Nanoparticles for Theranostic Applications. *Chemistry* **2013**, *19*, 6122–6136.
22. Rima, W.; Sancey, L.; Aloy, M. T.; Armandy, E.; Alcantara, G. B.; Epicier, T.; Malchere, A.; Joly-Pottuz, L.; Mowat, P.; Lux, F.; *et al.* Internalization Pathways into Cancer Cells of Gadolinium-Based Radiosensitizing Nanoparticles. *Biomaterials* **2013**, *34*, 181–195.
23. Sancey, L.; Lux, F.; Kotb, S.; Roux, S.; Dufort, S.; Bianchi, A.; Cremillieux, Y.; Fries, P.; Coll, J. L.; Rodriguez-Lafrasse, C.; *et al*. The Use of Theranostic Gadolinium-Based Nanoprobes to Improve Radiotherapy Efficacy. *Br. J. Radiol.* **2014**, 14–00134.
24. Bridot, J. L.; Faure, A. C.; Laurent, S.; Riviere, C.; Billotey, C.; Hiba, B.; Janier, M.; Josserand, V.; Coll, J. L.; Elst, L. V.; *et al*. Hybrid Gadolinium Oxide Nanoparticles: Multimodal Contrast Agents for *in Vivo* Imaging. *J. Am. Chem. Soc.* **2007**, *129*, 5076–5084.
25. Kryza, D.; Taleb, J.; Janier, M.; Marmuse, L.; Miladi, I.; Bonazza, P.; Louis, C.; Perriat, P.; Roux, S.; Tillement, O.; *et al*. Biodistribution Study of Nanometric Hybrid Gadolinium Oxide Particles as a Multimodal SPECT/MR/Optical Imaging and Theragnostic Agent. *Bioconjugate Chem.* **2011**, *22*, 1145–1152.
26. Miladi, I.; Duc, G. L.; Kryza, D.; Berniard, A.; Mowat, P.; Roux, S.; Taleb, J.; Bonazza, P.; Perriat, P.; Lux, F.; *et al*. Biodistribution of Ultra Small Gadolinium-Based Nanoparticles as Theranostic Agent: Application to Brain Tumors. *J. Biomater. Appl.* **2013**, *28*, 385–394.
27. Thomsen, H. S. Nephrogenic Systemic Fibrosis: A Serious Late Adverse Reaction to Gadodiamide. *Eur. Radiol.* **2006**, *16*, 2619–2621.
28. Truillet, C.; Lux, F.; Tillement, O.; Dugourd, P.; Antoine, R. Coupling of HPLC with Electrospray Ionization Mass Spectrometry for Studying the Aging of Ultrasmall Multifunctional Gadolinium-Based Silica Nanoparticles. *Anal. Chem.* **2013**, *85*, 10440–10447.
29. Bianchi, A.; Dufort, S.; Lux, F.; Courtois, A.; Tillement, O.; Coll, J. L.; Cremillieux, Y. Quantitative Biodistribution and Pharmacokinetics of Multimodal Gadolinium-Based Nanoparticles for Lungs Using Ultrashort TE MRI. *Magma* **2013**, *27*, 303–316.
30. Motto-Ros, V.; Negre, E.; Pelascini, F.; Panczer, G.; Yu, J. Precise Alignment of the Collection Fiber Assisted by Real-Time Plasma Imaging in Laser-Induced Breakdown Spectroscopy. *Spectrochim Acta, Part B* **2014**, *92*, 60–69.
31. Motto-Ros, V.; Sancey, L.; Ma, Q. L.; Lux, F.; Bai, X. S.; Wang, X. C.; Yu, J.; Panczer, G.; Tillement, O. Mapping of Native Inorganic Elements and Injected Nanoparticles in a Biological Organ with Laser-Induced Plasma. *Appl. Phys. Lett.* **2012**, *101*, 223702.
32. Sancey, L.; Motto-Ros, V.; Kotb, S.; Wang, X. C.; Lux, F.; Panczer, G.; Yu, J.; Tillement, O. Laser-Induced Breakdown Spectroscopy: A New Approach for Nanoparticle's Mapping and Quantification in Organ Tissue. *J. Vis. Exp.* **2014**, e51353.
33. Zipfel, W. R.; Williams, R. M.; Webb, W. W. Nonlinear Magic: Multiphoton Microscopy in the Biosciences. *Nat. Biotechnol.* **2003**, *21*, 1369–1377.
34. Pittet, M. J.; Weissleder, R. Intravital Imaging. *Cell* **2011**, *147*, 983–991.
35. Sancey, L.; Motto-Ros, V.; Busser, B.; Kotb, S.; Benoit, J. M.; Piednoir, A.; Lux, F.; Tillement, O.; Panczer, G.; Yu, J. Laser Spectrometry for Multi-elemental Imaging of Biological Tissues. *Sci. Rep* **2014**, *4*, 6065.
36. Abdelhalim, M. A.; Abdelmottaleb Moussa, S. A. The Gold Nanoparticle Size and Exposure Duration Effect on the Liver and Kidney Function of Rats. *In Vivo. Saudi J. Biol. Sci.* **2013**, *20*, 177–181.
37. Chromy, V.; Rozkosna, K.; Sedlak, P. Determination of Serum Creatinine by Jaffe Method and How To Calibrate To Eliminate Matrix Interference Problems. *Clin Chem. Lab Med.* **2008**, *46*, 1127–1133.
38. Ashworth, S. L.; Sandoval, R. M.; Tanner, G. A.; Molitoris, B. A. Two-Photon Microscopy: Visualization of Kidney Dynamics. *Kidney Int.* **2007**, *72*, 416–421.
39. He, X.; Nie, H.; Wang, K.; Tan, W.; Wu, X.; Zhang, P. *In Vivo* Study of Biodistribution and Urinary Excretion of Surface-Modified Silica Nanoparticles. *Anal. Chem.* **2008**, *80*, 9597–9603.
40. Popplewell, J. F.; King, S. J.; Day, J. P.; Ackrill, P.; Fifield, L. K.; Cresswell, R. G.; di Tada, M. L.; Liu, K. Kinetics of Uptake and Elimination of Silicic Acid by a Human Subject: A Novel Application of 32Si and Accelerator Mass Spectrometry. *J. Inorg. Biochem* **1998**, *69*, 177–180.
41. Le Duc, G.; Roux, S.; Paruta-Tuarez, A.; Dufort, S.; Brauer, E.; Marais, A.; Truillet, C.; Sancey, L.; Perriat, P.; Lux, F.; *et al*. Advantages of Gadolinium Based Ultrasmall Nanoparticles *vs* Molecular Gadolinium Chelates for Radiotherapy Guided by MRI for Glioma Treatment. *Cancer Nanotechnol.* **2014**, *5*.
42. Thadhani, R.; Pascual, M.; Bonventre, J. V. Acute Renal Failure. *New Engl. J. Med.* **1996**, *334*, 1448–1460.
43. Fujigaki, Y. Different Modes of Renal Proximal Tubule Regeneration in Health and Disease. *World J. Nephrol. Urol.* **2012**, *1*, 92–99.
44. Hagen, J. J.; Monning, C. A. Method for Estimating Molecular Mass from Electrospray Spectra. *Anal. Chem.* **1994**, *66*, 1877–1883.